

# Magnetic Properties of NiO Nano Particles: Contributions of the Antiferromagnetic and Ferromagnetic Subsystems in Different Magnetic Field Ranges up to 250 kOe

D. A. Balaev<sup>a, b, \*</sup>, A. A. Dubrovskiy<sup>a</sup>, A. A. Krasikov<sup>a</sup>, S. I. Popkov<sup>a, b</sup>, A. D. Balaev<sup>a</sup>,  
K. A. Shaikhutdinov<sup>a</sup>, V. L. Kirillov<sup>c</sup>, and O. N. Mart'yanov<sup>c</sup>

<sup>a</sup> Kirensky Institute of Physics, Federal Research Center KSC SB RAS, Krasnoyarsk, 660036 Russia

<sup>b</sup> Siberian Federal University, Krasnoyarsk, 660041 Russia

<sup>c</sup> Boreskov Institute of Catalysis, Russian Academy of Sciences, Siberian Branch, Novosibirsk, 630090 Russia

\*e-mail: dabalaev@iph.krasn.ru

Received February 14, 2017

**Abstract**—The magnetic properties of antiferromagnetic NiO nanoparticles prepared by thermal decomposition of nickel hydroxocarbonate are investigated. According to the data of magnetization measurements in fields of up to 250 kOe, the magnetic moment linearly grows in strong fields, which is caused by the contribution of the antiferromagnetically ordered nanoparticle core, and the antiferromagnetic susceptibility corresponds to that of bulk polycrystalline NiO. This allowed the antiferromagnetic and ferromagnetic contributions to the total magnetic response of a sample to be quantitatively determined. The latter occurs due to the incomplete spin compensation in an antiferromagnetic nanoparticle caused by defects on its surface. It is demonstrated that to correctly determine the superparamagnetic blocking temperature, it is necessary to take into account the antiferromagnetic susceptibility of the particle core.

DOI: 10.1134/S1063783417080029

## 1. INTRODUCTION

At present, nanoparticles of materials characterized by the antiferromagnetic (AFM) ordering have been intensively investigated to establish the fundamentals of variation in their magnetic properties caused by the size and surface effects, as well as defects and structural distortions [1–12]. The main difference of the magnetic properties of AFM nanoparticles from the bulk analogs is the occurrence of uncompensated magnetic moment  $\mu_{\text{unc}}$  in small particles [1, 3–8, 10–12]. As a result, a chemically and structurally homogeneous AFM nanoparticle contains at least two magnetic phases: the AFM phase of the particle core and ferromagnetic (FM) phase caused by the occurrence of  $\mu_{\text{unc}}$ . The presence of a magnetic moment of AFM nanoparticles opens the way for their application [13–15].

The magnetic properties of AFM nanoparticles are analyzed by the approaches conventionally used for describing ferri- and ferromagnetic particles: there are different temperature ranges of the blocked ( $T < T_B$ , where  $T_B$  is the blocking temperature) and unblocked ( $T > T_B$ ) states characterized by the presence and absence of magnetic hysteresis, respectively. The  $T_B$  value is determined from the well-known expression

$$T_B = KV / \ln(\tau/\tau_0)k_B, \quad (1)$$

where  $K$  is the magnetic anisotropy constant,  $V$  is the particle volume,  $k_B$  is the Boltzmann constant, and  $\tau$  and  $\tau_0$  are the characteristic times of measurement and relaxation of the particle magnetic moment. In this case,  $\tau_0 \approx 10^{-9} - 10^{-11}$  s and  $\tau \approx 10^1 - 10^2$  s for the quasi-static magnetic measurements, which yields  $T_B \approx KV/25k_B$ .

The magnetic response  $M_{\text{tot}}(H, T)$  of AFM particles can be described in the first approximation by the superposition of two contributions corresponding to the FM and AFM phases

$$M_{\text{tot}}(H, T) = M_{\text{FM}}(H, T) + M_{\text{AF}}(H, T). \quad (2)$$

At  $T > T_B$ , the FM contribution is simulated by the Langevin function with regard to the size or magnetic moment distribution of particles; at  $T < T_B$ , the magnetic hysteresis of the FM contribution is determined by the competition between the magnetic anisotropy energy  $KV$  and Zeeman energy  $\mu_{\text{unc}}\mathbf{H}$ . The magnetic field dependence of the AFM contribution is written in the form  $M_{\text{AF}}(H) = \chi_{\text{AF}}H$ , where  $\chi_{\text{AF}}$  is the AFM susceptibility of the AFM particle core. In this approach, the  $\chi_{\text{AF}}$  value should be comparable with the AFM susceptibility of the bulk material and the temperature dependence of  $\chi_{\text{AF}}$  should be analogous to the behavior of magnetic susceptibility of the bulk

antiferromagnet (as in the case of a polycrystal with the random crystallographic orientation of crystallites).

On the other hand, in small AFM particles, the additional AFM susceptibility growth can be observed, which was predicted by Neel [16–18] and is called superantiferromagnetism. This size effect consists in the fact that in AFM particles with the even number of FM planes the surface spins rotate under the action of field  $\mathbf{H}$  perpendicular to the easy magnetization axis stronger than the spins of internal planes. The noticeable increase in the AFM susceptibility can be observed in the particles that have no more than several dozen FM-ordered planes in diameter. However, as the size of AFM particles decreases, their uncompensated magnetic moment  $\mu_{\text{unc}}$  responsible for the FM phase starts playing an increasing role. As was shown by Neel [18], the  $\mu_{\text{unc}}$  value is determined as

$$\mu_{\text{unc}} \propto JN^b, \quad (3)$$

where  $N$  is the number of magnetically active atoms in a particle,  $J$  is the magnetic moment of an atom, and exponent  $b$  takes the values between  $1/3$ – $2/3$ , depending on the character of defects in a particle ( $b = 1/3$  corresponds to defects on the particle surface). Separation of the AFM and FM contributions in accordance with the results of magnetic measurements of small AFM particles is a nontrivial problem. The fact is that in the conventionally investigated magnetic field range of up to 60–90 kOe, the contribution of small magnetic moments can be still far from saturation, which complicates the unambiguous separation of the AFM contribution from the magnetization curve. In this case, it is reasonable to use strong pulsed magnetic fields, which essentially broadens the measurement range of magnetization curves.

Silva et al. [19] showed that the anomalous  $\chi_{\text{AF}}(T)$  dependence of AFM-ordered ferritin, specifically, a decrease in the  $\chi_{\text{AF}}$  value with increasing  $T$  obtained by many authors [1, 6, 20–23] by processing the  $M(H)$  dependences in fields of up to 60 kOe, is most likely an artefact. In sufficiently strong ( $\sim 200$  kOe) fields, the  $\chi_{\text{AF}}$  values obtained from the derivative  $dM/dH$  are noticeably smaller, whereas the  $\chi_{\text{AF}}(T)$  dependence at  $H > 200$  kOe is already classical, i.e., increases with temperature. Among different AFM nanoparticle materials, studies in strong pulsed fields were carried out only for ferritin [18, 24, 25] and lanthanum manganite [26]. Therefore, it would be reasonable to investigate other AFM nanoparticles using this technique. In this study, we present the results of investigation of the magnetic properties of nickel oxide nanoparticles. At the first stage, we study the sample with relatively coarse particles ( $\sim 25$  nm on average), where the superantiferromagnetism effect should be insignificant.

## 2. EXPERIMENTAL

### 2.1. Fabrication and Characterization of the Samples

NiO nanoparticles were prepared by thermal decomposition of nickel hydroxycarbonate  $\text{NiCO}_3 \cdot 0.18\text{Ni}(\text{OH})_2 \cdot 0.50\text{H}_2\text{O}$  (basic nickel carbonate). The heating was performed at  $90^\circ\text{C}$  for 14 h; after that, the temperature was increased to  $500^\circ\text{C}$  for 5 h and the sample was exposed at this temperature for 1 h. This sample is referred to as nano-NiO.

The diffraction pattern for the nano-NiO sample was obtained on a Bruker D8 Advance device in  $\text{CuK}\alpha$  radiation ( $\lambda = 1.5418 \text{ \AA}$ ). The results are presented in Fig. 1. All the observed diffraction peaks belong to the NiO phase (PDF no. 047-1049). The NiO cubic unit cell parameter coincides with a standard value (sp. gr.  $Fm\bar{3}m$ ,  $a = b = c = 4.176 \text{ \AA}$ ,  $\alpha = \beta = \gamma = 90^\circ$ ). The coherent scattering region size determined from the broadening of diffraction peaks is about 30 nm.

Microphotographs of the nano-NiO sample particles were obtained by high-resolution transmission electron microscopy (HRTEM) on a JEOL JEM-2010 microscope with a resolution of  $1.4 \text{ \AA}$  at an accelerating voltage of 200 kV. Figure 2 shows typical HRTEM data for the nano-NiO sample. The average NiO nanoparticle size, according to several microphotographs, is 25 nm, which is similar to the coherent scattering region size.

For comparison, we studied the magnetic properties of the bulk polycrystalline nickel oxide sintered in a tablet at  $600^\circ\text{C}$  from the NiO reactive. This sample is referred to as bulk NiO.

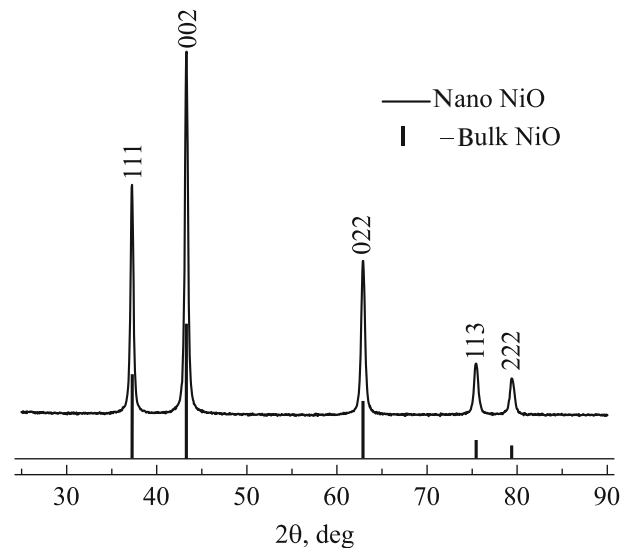


Fig. 1. Experimental diffraction pattern of the nano-NiO sample in comparison with the bar diagram illustrating the position and relative intensity of the NiO phase peaks.

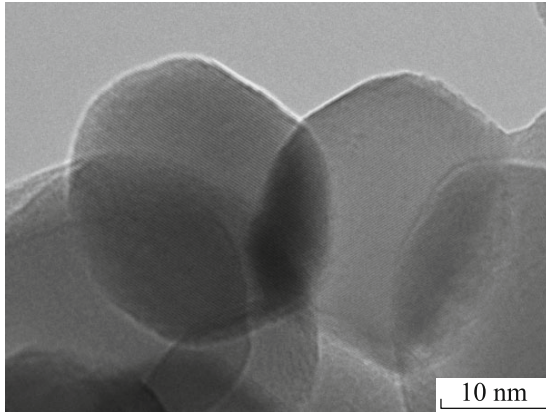


Fig. 2. HRTEM data for the nano-NiO sample.

### 2.2. Measurements of the Magnetic Properties

The quasi-static magnetic measurements were performed on a vibrating sample magnetometer (VSM) [27]. The investigated powder was fixed in a measuring capsule in paraffin. The temperature dependences of the magnetic moment  $M(T)$  were measured in the zero field cooling (ZFC) mode and in an external field (FC). The magnetization curves  $M(H)$  were measured in pulsed magnetic fields on a setup at the Kirensky Institute of Physics (Krasnoyarsk). The investigated powder (64 mg) was securely fixed in an induction sensor of the pulsed magnetometer. The pulse length was 16 ms. Magnetization isotherms were measured at a temperature of 77.4 K and magnetic field pulse amplitudes of up to 250 kOe.

## 3. RESULTS AND DISCUSSION

Figure 3a shows temperature dependences of the magnetic moment for the nano-NiO sample obtained in fields of  $H = 1$  kOe (ZFC and FC modes), 10 kOe (ZFC mode), and 60 kOe (obtained from the  $M(H)$  isotherms (see below)). The data in Figs. 3a and 3b are given in emu/g units (magnetic moment of the unit sample mass) divided by the external field, i.e.,  $M(T)/H$ . In addition, Fig. 3a shows the  $M(T)/H$  dependence for the bulk NiO sample in an external field of 1 kOe. For this sample, as expected for bulk AFM polycrystalline materials, the dependence  $M(H) = \chi_{AF}H$  is the linear hysteresisless function; no thermomagnetic prehistory effects are observed. Hence, the  $M(T)/H$  dependence for the bulk NiO sample corresponds to the temperature behavior of the AFM susceptibility of bulk polycrystalline nickel oxide ( $M(T)/H = \chi_{AF}(T)$ ) with a Neel temperature of 523 K [28].

As applied to the data in Fig. 3a, expression (2) is rewritten in the form

$$M_{\text{tot}}(T)/H = M_{\text{FM}}(T)/H + \chi_{\text{AF}}(T). \quad (4)$$

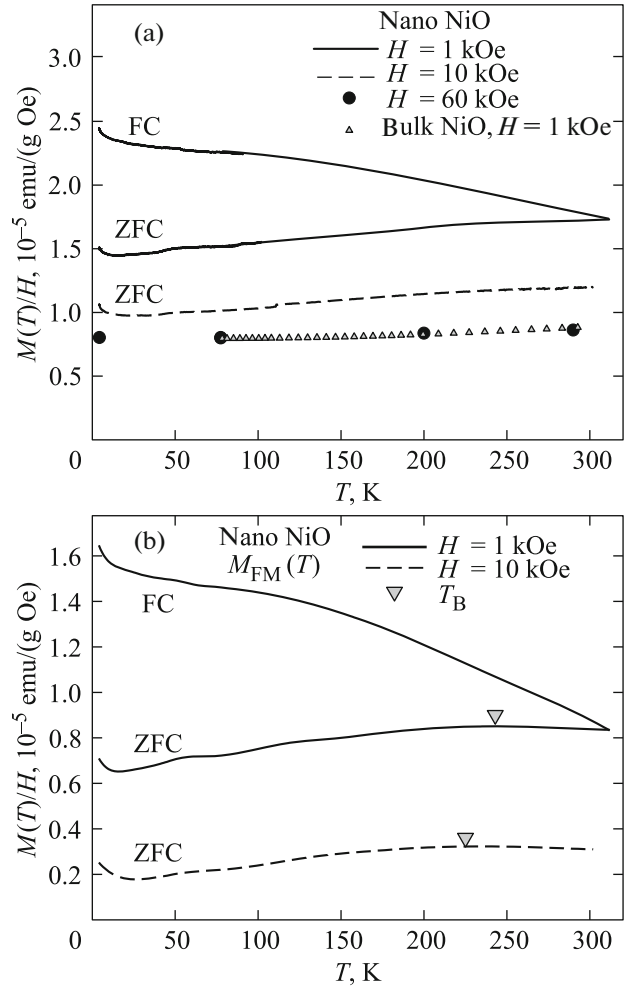
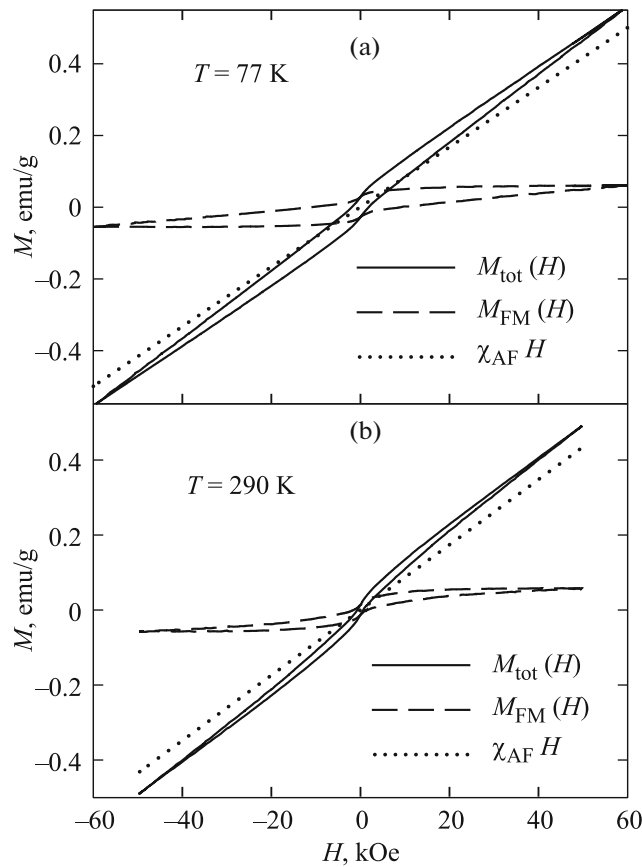


Fig. 3. Temperature dependences of the magnetic moment  $M(T)/H$  for the nano-NiO sample in external fields of 1 and 10 kOe and the  $M(H = 60 \text{ kOe})/60 \text{ kOe}$  values at different temperatures. (b)  $M(T)/H$  dependences for the FM subsystem of the nano-NiO sample in fields of 1 and 10 kOe after subtracting the AF component according to (4). The maximum temperature  $T_B$  of the  $M_{\text{FM}}(T)$  under the ZFC conditions.

It can be seen in Fig. 3a that the largest difference between the data for polycrystalline and nanosized NiO corresponds to  $H = 1$  kOe; at  $H = 60$  kOe the  $M(T)/H$  dependence for the nano-NiO sample almost coincides with  $\chi_{\text{AF}}(T)$  of the bulk NiO sample. This is explained by the contribution of the first term of Eq. (4), which saturates in strong fields (in saturation,  $M_{\text{FM}} \approx \text{const}$  and  $dM_{\text{FM}}(H)/dH \approx 0$ ).

Let us consider the evolution of the  $M(T)$  dependences for the nano-NiO sample. It can be seen that the ZFC  $M(T)$  dependences monotonically increase with temperature above 30 K. The  $M(T)$  dependence in a field of  $H = 1$  kOe tends to saturation at temperatures near 250 K. It would be reasonable to attribute this to the maximum in the ZFC  $M(T)$  dependence,



**Fig. 4.** Hysteretic  $M_{\text{tot}}(H)$  dependences for the nano-NiO sample, straight  $\chi_{\text{AF}}H$  corresponding to the AF contribution, and hysteretic  $M_{\text{FM}}(H)$  dependences (see Eq. 5) corresponding to the FM contribution at temperatures of (a)  $T = 77$  and (b) 290 K.

i.e., to the characteristic blocking temperature  $T_B$  of superparamagnetic particles. As the external field is increased, the blocking temperature should shift toward lower temperatures. However, the data on the nano-NiO sample do not confirm this: on the contrary, the  $M(T)$  dependence at  $H = 10$  kOe is the increasing function without saturation.

On the other hand, according to Eq. (4), the FM contribution can be separated by subtracting the AFM component. The plots in Fig. 3b were obtained by subtracting the experimental  $\chi_{\text{AF}}(T)$  data for the bulk NiO sample from the corresponding  $M(H)/H$  dependences for the nano-NiO sample. The obtained  $M_{\text{FM}}(T)/H$  dependences for the FM subsystem are typical of superparamagnetic systems: as the field increases, the pronounced ZFC  $M_{\text{FM}}(T)$  maximum at blocking temperature  $T_B$  shifts to the low-temperature region to  $\sim 245$  K at  $H = 1$  kOe and to  $\sim 225$  K at  $H = 10$  kOe.

At a magnetic anisotropy constant of  $K \approx 0.8 \times 10^5$  erg/cm<sup>3</sup> of bulk NiO [28], the value of  $T_B \approx 245$  K corresponds, according to Eq. (1), to the particles

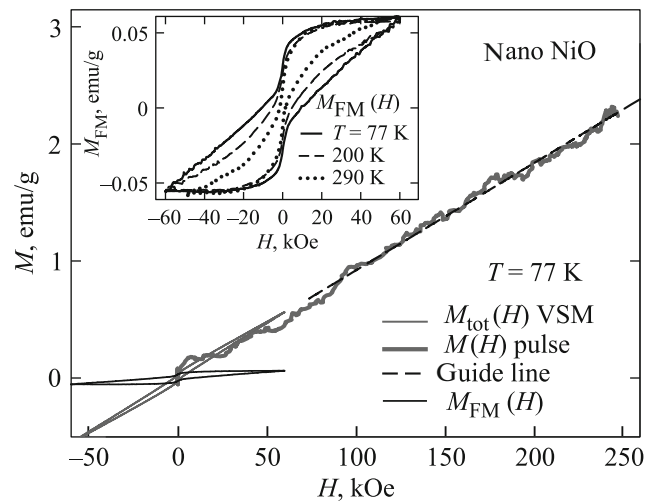


**Fig. 5.**  $M_{\text{tot}}(H)$  magnetization curve for the nano-NiO sample in a pulsed field of up to 250 kOe and VSM data (up to 60 kOe) at  $T = 77$  K. FM contribution  $M_{\text{FM}}(H)$  to the total magnetization curve. Inset:  $M_{\text{FM}}(H)$  dependences at different temperatures.

$\sim 23$  nm in size. This agrees well with the nano-NiO sample particle size determined by HRTEM ( $\sim 25$  nm). Note that this  $T_B$  value approximately corresponds to the average particle size and the irreversible behavior of the  $M(T)$  dependences and  $M(H)$  hysteresis in the temperature range of  $T > T_B$  (see below) are determined by the largest particles in accordance with the size distribution. Thus, the temperature behavior of the AFM susceptibility of the nanoparticle core can significantly affect determination of their blocking temperatures, which is shown first in this study.

Figures 4a and 4b show hysteretic  $M(H)$  dependences for the nano-NiO sample at temperatures of 77 and 290 K, respectively. Their character unambiguously evidence for the coexistence of two investigated magnetic subsystems and superposition of their magnetic responses to the total magnetization curve  $M_{\text{tot}}(H)$ :

$$M_{\text{tot}}(H) = M_{\text{FM}}(H) + \chi_{\text{AF}}H. \quad (5)$$

For the FM subsystem, the saturation is expected, which should be confirmed by the linear character of the  $M_{\text{tot}}(H)$  dependence in sufficiently strong magnetic fields. Figure 5 shows the data for the nano-NiO sample in a pulsed magnetic field of up to 250 kOe together with the VSM data in the range of up to 60 kOe. It can be seen from Fig. 5 that the  $M_{\text{tot}}(H)$  dependence is linear with respect to the field in the investigated field range. Consequently, the contribution of the FM subsystem saturates, at least at temperatures above  $\sim 77$  K. The slope of the  $M_{\text{tot}}(H)$  dependence in fields over  $\sim 100$  kOe agrees well with

the  $\chi_{AF}$  value for the bulk NiO sample (Fig. 3a) at a measuring temperature of 77 K.

The straights in Figs. 4a and 4b correspond to the contribution of the AF subsystem ( $\chi_{AF}H$ ) at the  $\chi_{AF}$  values determined from the  $M(T)/H$  dependence of the bulk NiO sample (Fig. 3a). Subtracting the AF contribution from the total sample magnetization, we can obtain the  $M_{FM}(H)$  dependences from Eq. (5):  $M_{FM}(H) = M_{tot}(H) - \chi_{AF}H$ . These dependences are presented in Figs. 4a and 4b and the inset in Fig. 5. It can be seen that the  $M_{FM}(H)$  dependences tend to saturation in the field range of up to  $\sim 60$  kOe; the coercivity decreases with increasing temperature.

The saturation magnetization of the FM subsystem (see inset in Fig. 5) is  $\sim 0.06$  emu/g. At a magnetic moment of  $Ni^{2+} \approx (2-2.3)\mu_B$  in NiO [5], this value corresponds to a fraction of uncompensated spins of  $\sim (4 \times 10^{-4})$  of all nickel atoms in the oxide. According to model hypothesis (3), the number of uncompensated spins for a particle  $\sim 25$  nm in size is about 80 at  $b = 1/3$ , which corresponds to a fraction of  $\sim (1.5 \times 10^{-4})$  of all Ni atoms in a particle of this size. For a 25-nm particle, the  $\mu_{unc}$  value is about  $430\mu_B$ , according to the experimental  $M_{FM}(H)$  saturation value and  $170\mu_B$ , according to model hypothesis (3) at  $b = 1/3$ . It can be seen that the Neel model hypothesis is in good agreement with the experiment in the order of magnitude of uncompensated magnetic moments in NiO. This indicates that the FM contribution is caused by defects on the particle surface.

Note that at a temperature of 4.2 K, the above procedure of separation of the FM and AFM contributions did not allow us to obtain the  $M_{FM}(H)$  dependence saturating in field of about 60 kOe. Let us point out two reasons that prevent separation of these contributions. First, Eq. (2) suggests that the FM and AFM contributions are independent. However, the AFM and FM subsystems can be exchange-coupled, which should lead, in particular, to the observed exchange shift of the hysteresis loop after cooling in an external field. This was observed for NiO [4, 29, 30] and other AFM nanoparticles [31–35]. As a rule, the exchange shift decreases at high temperatures [4, 12, 30], which allows the AF nanoparticle to be considered as two independent subsystems. In the low-temperature region, the exchange coupling of the AFM and FM subsystems apparently leads to the slower saturation of the latter with increasing field. Second, magnetically ordered nanoparticles almost always contain surface spins, which are not exchange-coupled with the inner spins [2, 12, 35–40]. At low temperatures, this additional subsystem exhibits the spin glasslike behavior and, as the temperature increases, behaves as a paramagnetic phase (noninteracting spins). The noticeable growth of the magnetic moment with decreasing temperature in the range below 30 K observed in the nano-NiO sample (Fig. 3)

is indicative of the presence of this additional spin glasslike subsystem of surface atoms. As the temperature grows, the contribution of this subsystem to the resulting magnetic response of nanoparticles becomes negligible (decreases proportionally to  $\propto 1/T$ ), which allows the AFM and FM contributions to be unambiguously separated.

## CONCLUSIONS

Based on the investigated magnetic properties of NiO nanoparticles in magnetic fields of up to 250 kOe, we demonstrated that the magnetic contribution (magnetic susceptibility  $\chi_{AF}$ ) of the AFM-ordered core of nanoparticles  $\sim 25$  nm in size agrees well with the behavior of bulk AFM NiO. This makes it possible to separate the AFM and FM contributions in a wide temperature range (at least, above  $\sim 70$  K). The FM contribution is caused by defects on the particle surface and the uncompensated moment is consistent with the model representations proposed by Neel. The account for the temperature behavior of the AFM susceptibility  $\chi_{AF}(T)$  of the particle core is needed to correctly determine the superparamagnetic blocking temperature of particles, which is  $\sim 245$  K in a field of  $H = 1$  kOe for the investigated sample. At low temperatures, one can observe the contribution of one more magnetic subsystem, i.e., a part of surface spins, which are not exchange-coupled with the AFM core.

## ACKNOWLEDGMENTS

This study was supported by the Russian Foundation for Basic Research, Government of the Krasnoyarsk Territory, and Krasnoyarsk Territorial Foundation for Support of Scientific and R&D Activity, project no. 17-42-240138.

## REFERENCES

1. S. Mørup, D. E. Madsen, C. Fradsen, C. R. H. Bahl, and M. F. Hansen, *J. Phys.: Condens. Matter* **19**, 213202 (2007).
2. R. H. Kodama and A. E. Berkowitz, *Phys. Rev. B* **59**, 6321 (1999).
3. Yu. L. Raikher and V. I. Stepanov, *J. Phys.: Condens. Matter* **20**, 204120 (2008).
4. S. A. Makhlof, F. T. Parker, F. E. Spada, and A. E. Berkowitz, *J. Appl. Phys.* **81** 5561 (1997).
5. S. D. Tiwari and K. P. Rajeev, *Solid State Commun.* **152**, 1080 (2012).
6. S. A. Makhlof, F. T. Parker, and A. E. Berkowitz, *Phys. Rev. B* **55**, R14717 (1997).
7. D. A. Balaev, A. A. Krasikov, A. A. Dubrovskiy, S. I. Popkov, S. V. Stolyar, R. S. Iskhakov, V. P. Ladygina, and R. N. Yaroslavtsev, *J. Appl. Phys.* **120**, 183903 (2016).
8. A. A. Lepeshev, I. V. Karpov, A. V. Ushakov, D. A. Balaev, A. A. Krasikov, A. A. Dubrovskiy, D. A. Veli-

- kanov, and M. I. Petrov, *J. Supercond. Nov. Magn.* (2016). doi 10.1007/s10948-016-3885-4
9. Yu. A. Kumzerov, N. F. Kartenko, L. S. Parfen'eva, I. A. Smirnov, A. A. Sysoeva, H. Misiorek, and A. Jezowski, *Phys. Solid State* **54**, 1066 (2012).
  10. D. A. Balaev, A. A. Krasikov, A. A. Dubrovskiy, S. I. Popkov, S. V. Stolyar, O. A. Bayukov, R. S. Iskhakov, V. P. Ladygina, and R. N. Yaroslavtsev, *J. Magn. Magn. Mater.* **410**, 71 (2016).
  11. D. A. Balaev, A. A. Krasikov, A. A. Dubrovskii, S. V. Semenov, O. A. Bayukov, S. V. Stolyar, R. S. Iskhakov, V. P. Ladygina, and L. A. Ishchenko, *J. Exp. Theor. Phys.* **119**, 479 (2014).
  12. A. Punnoose, H. Magnone, M. S. Seehra, and J. Bonnevich, *Phys. Rev. B* **64**, 174420 (2001).
  13. Q. A. Pankhurst, N. T. K. Thanh, S. K. Jones, and J. Dobson, *J. Phys. D* **42**, 224001 (2009).
  14. Q. A. Pankhurst, J. Connolly, S. K. Jones, and J. Dobson, *J. Phys. D* **36**, R167 (2003).
  15. K. Dobretsov, S. Stolyar, and A. Lopatin, *Acta Otorhinolaryngol. Ital.* **35**, 97 (2015).
  16. L. Néel, *C.R. Acad. Sci. Paris* **253**, 1286 (1961).
  17. L. Néel, *C.R. Acad. Sci. Paris* **253**, 203 (1961).
  18. L. Néel, *C.R. Acad. Sci. Paris* **252**, 4075 (1961).
  19. N. J. O. Silva, A. Millan, F. Palacio, E. Kampert, U. Zeitler, and V. S. Amaral, *Phys. Rev. B* **79**, 104405 (2009).
  20. M. S. Seehra, V. S. Babu, A. Manivannan, and J. W. Lynn, *Phys. Rev. B* **61**, 3513 (2000).
  21. A. Punnoose, T. Phanthavady, M. S. Seehra, N. Shah, and G. P. Huffman, *Phys. Rev. B* **69**, 054425 (2004).
  22. N. J. O. Silva, V. S. Amaral, and L. D. Carlos, *Phys. Rev. B* **71**, 184408 (2005).
  23. M. S. Seehra, V. Singh, X. Song, S. Bali, and E. M. Eyring, *J. Phys. Chem. Solids* **71**, 1362 (2010).
  24. R. P. Guertin, N. Harrison, Z. X. Zhou, S. McCall, and F. Drymiotis, *J. Magn. Magn. Mater.* **308**, 97 (2007).
  25. C. Gilles, P. Bonville, H. Rakoto, J. M. Broto, K. K. W. Wong, and S. Mann, *J. Magn. Magn. Mater.* **241**, 430 (2002).
  26. V. Markovich, R. Puzniak, Y. Skourski, A. Wisniewski, D. Mogilyanski, G. Jung, and G. Gorodetsky, *J. Phys.: Condens. Matter* **24**, 266001 (2012).
  27. A. D. Balaev, Yu. V. Boyarshinov, M. M. Karpenko, and B. P. Khrustalev, *Prib. Tekh. Eksp.*, No. 3, 167 (1985).
  28. M. Tadic, D. Nikolic, M. Panjan, and G. R. Blake, *J. Alloys Compd.* **647**, 1061 (2015).
  29. S. A. Makhlof, H. Al-Attar, and R. H. Kodama, *Solid State Commun.* **145**, 1 (2008).
  30. M. S. Seehra and A. Punnoose, *Solid State Commun.* **128**, 299 (2003).
  31. A. Punnoose and M. S. Seehra, *J. Appl. Phys.* **91**, 7766 (2002).
  32. C. Diaz-Guerra, M. Vila, and J. Piqueras, *Appl. Phys. Lett.* **96**, 193105 (2010).
  33. D. A. Balaev, A. A. Krasikov, A. A. Dubrovskiy, S. V. Semenov, S. I. Popkov, S. V. Stolyar, R. S. Iskhakov, V. P. Ladygina, and R. N. Yaroslavtsev, *Phys. Solid State* **58**, 287 (2016).
  34. N. J. O. Silva, V. S. Amaral, A. Urtizberea, R. Bustamante, A. Millán, F. Palacio, E. Kampert, U. Zeitler, S. de Brion, O. Iglesias, and A. Labarta, *Phys. Rev. B* **84**, 104427 (2011).
  35. S. Giri, M. Patra, and S. Majumdar, *J. Phys.: Condens. Matter* **23**, 073201 (2011).
  36. V. L. Kirillov, D. A. Balaev, S. V. Semenov, K. A. Shaykhtudinov, and O. N. Martyanov, *Mater. Chem. Phys.* **145**, 75 (2014).
  37. Yu. A. Koksharov, S. P. Gubin, I. D. Kosobudsky, G. Yu. Yurkov, D. A. Pankratov, L. A. Ponomarenko, M. G. Mikheev, M. Beltran, Y. Khodorkovsky, and A. M. Tishin, *Phys. Rev. B* **63**, 012407 (2000).
  38. D. A. Balaev, A. A. Dubrovskiy, K. A. Shaykhtudinov, O. A. Bayukov, S. S. Yakushkin, G. A. Bukhtiyarova, and O. N. Martyanov, *J. Appl. Phys.* **114**, 163911 (2013).
  39. A. A. Dubrovskiy, D. A. Balaev, K. A. Shaykhtudinov, O. A. Bayukov, O. N. Pletnev, S. S. Yakushkin, G. A. Bukhtiyarova, and O. N. Martyanov, *J. Appl. Phys.* **118**, 213901 (2015).
  40. K. Nadeem, H. Krenn, T. Traussnig, R. Würschum, D. V. Szabo, and I. Letofsky-Papst, *J. Appl. Phys.* **111**, 113911 (2012).

*Translated by E. Bondareva*